Interface Reactions in Fine-Grained Al_2O_3-Ceramics with TiO_2- and ZrO_2-Additions for Refractory Applications as Investigated by XCT and EBSD

H. Berek, Chr. G. Aneziris, D. Veres

Fine-grained Al_2O_3-ceramics with TiO_2- and ZrO_2-additions (AZT) exhibit superior thermal shock performance. Impressive results could be shown using bending tests before and after a thermal shock. The reasons for this behaviour have to be investigated in the microstructure. In the present paper the combined possibilities of X-Ray computed tomography (XCT) and electron backscatter diffraction (EBSD) for characterizing the microstructure of AZT materials are demonstrated.

1 Introduction

High alumina containing materials are established refractories with high refractoriness under load as well as excellent corrosion resistance in steel/slag environments. In spite these excellent properties, due to their poor thermal shock performance they are commonly used in combination with carbon for functional components such as submerged entry nozzles, slide gates etc. [1]. The common basic principle and motivation to investigate the Al_2O_3-TiO_2-ZrO_2-system is the microcrack formation and its contribution to both tailored thermal expansion behavior and thermal shock performance. The combination of Al_2O_3 and TiO_2 leads to the formation of Al_2TiO_5 that exhibits the highest R_1 thermal shock parameter according to *Hasselman* among all other ceramics [2–4]. Within the pseudo ternary alumina-titania-zirconia system two basic compounds exist, namely aluminum titanate and zirconium titanate [5]. The zirconium titanate composition ranges from $ZrTiO_4$ over $Zr_5Ti_7O_{24}$ up to $ZrTi_2O_6$ (Srilankite), i.e. from zirconia titania ratio of 1:1 to 1:2. Complete solid solubility between the first two compounds appears [6, 7]. Aluminum titanate occurs only in the form of Al_2TiO_5. Depending on the temperature the formation of either aluminum titanate or zirconium titanate is favored. Sintering of Al_2TiO_5-$ZrTiO_4$ composites at higher temperatures leads to a two phase microstructure, i.e. both components coexist [8]. A very interesting approach to study the thermal expansion behaviour of ceramic composites in the system Al_2O_3-ZrO_2-TiO_2 has been presented by *Virro-Nic* and *Pilling* [9]. Compositions were prepared from blended mixtures of oxide powders (Al_2O_3, *Aldrich*, purity 99,8 %, particle size <10 µm; TiO_2, *Johnson-Matthey*, purity >99 %, particle size 1,5–2,0 µm; ZrO_2, *Johnson-Matthey*, purity >99 %, –325 mesh), which were compacted into cylindrical rods and then melted in a tungsten arc-image furnace. They demonstrated that compositions of 20 mol-% Al_2O_3, 20 mol.-% ZrO_2 and 60 % TiO_2 present a thermal expansion coefficient of $-4{,}18\cdot10^{-6}$/K. A composition based on 40 mol-% TiO_2, 40 mol-% ZrO_2 and 20 mol-% Al_2O_3 reaches a thermal expansion coefficient of $0{,}5\cdot10^{-6}$/K, whereby 100 mol-% Al_2O_3 presents a thermal expansion coefficient of $8{,}6\cdot10^{-6}$/K, 100 mol-% $ZrTiO_4$ of $7{,}3\cdot10^{-6}$ and 100 mol-% Al_2TiO_5 of $-3{,}5\cdot10^{-6}$/K.

In a previous work thermal shock resistant honeycombs based on a doped alumina porous matrix have been described [10]. The additions of TiO_2 and Mg-PSZ to the alumina led to higher shrinkages but also contributed to grain growth in comparison to pure alumina materials. Besides Al_2O_3 grains three additional zones were identified in the doped alumina material due to EDX-Analyses. According to a model approach dealing with the thermal expansion coefficients of the different zones it was concluded that areas with a positive thermal expansion coefficient and those with a negative thermal expansion coefficient exist at Al_2O_3 grain boundaries. This structure leads to an improved thermal shock performance during heating up as well as cooling down. In [11] superior thermal shock performance of a carbon-free, fine grained low porous alumina ceramic with titania and zirconia additions was demonstrated and correlated to the generated microstructure. Thereby, the decomposition of the Al_2TiO_5 in the doped alumina matrix dominates during thermal shock attack and leads to higher strengths in comparison to the as sintered samples after thermal shock.

The goal of the present paper is a detailed phase analysis of the newly developed AZT materials with excellent thermo cycling properties by using XCT and EBSD in combination.

2 Experimental

Samples for the experimental methods such as determination of three point bending strength and thermal shock performance were prepared by slip casting. For the micro phase

Harry Berek, Christos G. Aneziris, Dániel Veres
TU Bergakademie Freiberg
Institute of Ceramic, Glass and Construction Materials
09596 Freiberg
Germany

Corresponding-Author: *H. Berek*
E-mail: harry.berek@ikgb.tu-freiberg.de

Keywords: Al_2O_3, ZrO_2, TiO_2, thermal shock, EBSD, XCT, microstructure

Received: 06.10.2011
Accepted: 25.10.2011

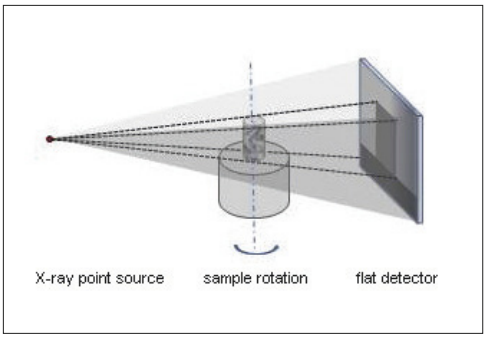

Fig. 1 XCT with the main parts of a cone configuration

analysis the materials have been manufactured using isostatic pressing. The raw materials were alumina Martoxid MR70 *(Martinswerk/DE)* with a d_{50} of 0,8 µm, magnesia partially stabilised zirconia with 3,4 mass-% MgO as stabilizing agent *(Saint Gobain/UK)* with a d_{50} of 1,3 µm and titania T-R *(Crenox/DE)* with a d_{50} of 1,0 µm. The compositions were mixed with de-ionized water with a weight ratio powder/water of 75/25. Organic additives were 0,3 mass-% Dispex A40 *(Ciba/DE)* and 0,15 mass-% Optapix AC170 *(Zschimmer & Schwarz/DE)* related to the solids. All components were mixed and homogenized in a polyethylene chamber with alumina milling media for five hours. The prepared slip was casted in plaster moulds of 3 mm × 4 mm × 45 mm sample dimensions, demoulded after 5 h and dried at 120 °C. Model components in the form of round rods were prepared by isostatic pressing. The materials were pressed with 80 MPa. The processing procedure was as follows: in the first step zirconia samples has been prepared. Around the sample, titania powder were filled and pressed again. In the last step, the alumina powder was filled around the zirconia titania sample and final isostatic pressing took place. There was no pressing additive used. Both kind of samples were sintered at 1650 °C with a heating rate of 2 K/min and a holding time of 2 h in an electrical furnace *(Nabertherm* HT 21/18*)* in oxidizing atmosphere.

Microstructure characterisation was conducted using X-ray computed tomography (XCT) and scanning electron microscopy (SEM) in combination with energy dispersive X-ray microanalysis (EDX) as well as electron backscatter diffraction (EBSD). The XCT experiments were performed in a CT-ALPHA from ProCon X-Ray *(Garbsen/DE)* using a 160 kV transmission X-ray tube from *Feinfocus Garbsen/DE*. There are a rising number of publications regarding the application of XCT in materials science (see [12–14]). We used the cone beam configuration. The experimental setup corresponds to Fig 1. High-resolution X-ray absorption images are taken with a flat detector C7942SK-05 from *Hamamatsu/JP*. This detector has 2400 x 2400 pixels with a size of 50 µm × 50 µm each on an area 120 mm × 120 mm. The resulting spatial resolution (voxel size) within the samples depends on geometry. We found 8,4 µm for AZT bending samples and 37,4 µm for the AZT model components. Typically images are taken at 400 steps between 0° and 360° sample rotation respectively. As the result of a reconstruction the spatial distribution of the voxel X-ray attenuation coefficients in relative grey levels is given. Note that a precondition for successful investigations in a XCT is the transferability of the sample in the full scan range between 0° and 360° respectively.

Overviews regarding the EBSD method are given in several contributions [15, 16]. Electron backscatter patterns (EBSP) contain all information about the lattice symmetry within the excited sample volume (about 20 to 100 nm in depth) and thus can be used for phase analysis. They consist of parallel lines for each reflecting lattice plane. The angles between these lines exactly correspond to the angle in the lattice structure. The analysis is realized by comparing the measured angles with those of known crystalline phases. The investigation was carried out in a conventional W-cathode scanning electron microscope *Philips XL30* equipped with an EBSD system TSL and an EDX system Genesis in connection with an Apollo10 detector from *Edax/Ametek*. Phase determination can be carried out for single spots or for defined scans. There are two preconditions for a successful EBSD phase mapping. First of all undisturbed and electrically conducting sample surfaces are needed. Sample preparation thus is of great importance especially in the case of multi crystalline ceramic materials, which contain a high number of cracks. The sample preparation was realized by 20 h vibration polishing in a *BUEHLER VibroMet2* using the *Buehler* suspension *MasterMet2* (0,02 µm silica). All samples were coated with Pt-layers in the range of 0,1 nm using a conventional sputter coater from *Cressington*.

The layer thickness is the result of an optimization process. On the one hand the layers have to be thick enough in order to avoid charging effects. On the other hand they have to be thin enough in order not to disturb the diffraction patterns. The second problem to be solved is a set of lattice parameters of phases, which really are involved in the given sample. An ICDD data base [17] was used. By comparing the EBSD results with X-ray diffraction a set of possible crystal structures was defined. The results for the given AZT materials are given in Tab. 1.

Tab. 1 Lattice parameters used in the EBSD phase analysis

Phase	ICDD No.	Crystal system	Lattice parameters					
			a [Å]	b [Å]	c [Å]	α [deg]	β [deg]	γ [deg]
α-Al_2O_3	0893072	trigonal	4,760	4,760	12,99	90	90	120
ZrO_2	0780047	monoclinic	5,1507	5,2038	5,3156	90	99,196	90
TiO_2	0760324	tetragonal	4,6452	4,6452	3,0017	90	90	90
$ZrTiO_4$	0340415	orthorhombic	5,0358	5,4874	4,8018	90	90	90
Al_2TiO_5	0410258	orthorhombic	9,439	9,647	3,5929	90	90	90

3 Results and discussion

The investigated AZT bending test samples exhibited excellent thermo cycling stability. In [10] it was stated that the properties of this materials can be explained with the formation of micro cracks in the Al_2O_3 inter granular regions. In these regions phases with different chemical compositions were found. According to [9] they have different CTE. In the frame of the present work combined XCT and EBSD investigations were carried out in order to further characterise the inter granular regions. X-ray computed tomography enables a quick overview to the structure without destroying the sample. However unfortunately the grey levels do not give the possibility to distinguish between different phases directly. A calibration becomes necessary. Fig. 2 shows the XCT image of an AZT model component. The diameter is 3 cm. The voxel size was 37,4 µm. Note that this model sample was manufactured using the same technology as for bending

samples. A calculated cross section also is given in Fig. 2. Obviously there are different grey levels within the regions of the sample. As a result of different CTE cracks appeared during the cooling process after sintering. Grey level histograms indicate the distribution of X-ray attenuation coefficients within the investigated sample. This kind of diagram is given in Fig. 3. The surrounding of the sample plus air in pores and cracks give rise for the left hand peak. A second peak arises because of epoxy, which was used in order to stabilise the sample. The third peak is a result of the overlapping from the Al_2O_3, ZrO_2 and TiO_2 absorption peaks respectively. By the help of histograms, calculated from partial volumes, this overlapping can be demonstrated. In Fig. 4 the resulting histogram from the partial volume outlined in Fig. 2 is shown. The contributions of Al_2O_3 and TiO_2 clearly can be seen. Fig. 5 gives the histogram of an AZT bending sample. A partial volume was calculated in order to minimise the influence of the surrounding and surface. Because of the given concentrations, the resulting peak is mainly determined by Al_2O_3. The very left wing to zero must be determined by cracks and holes within the sample volume. If regions of interest are calculated using only signals from this interval the distribution of cracks and holes can be represented. This is demonstrated in the Figs. 6, 7 for typical bending samples before and after thermal shock treatment (5 thermo shocks from 1200 °C). Note that the voxel size was 8,4 µm. A region of higher density of pores in the very middle of the samples clearly can be recognised in the transparent presentation and even so in the calculated cross section. Furthermore a network of fine cracks possibly micro cracks appeared after thermal cycling. This might be the reason for the good thermal stability of the samples. In order to clarify the microstructure cross sections of the bending samples were investigated by EBSD. Fig. 8 gives the SEM picture of a typical area in the middle of the sample and corresponding EDX elemental maps. Indeed there are pores filled with epoxy in the frame of the sample preparation. This is indicated by the carbon distribution. Fig. 9 shows a typical SEM picture from the bulk of an AZT bending sample and corresponding EBSD results. Note that in spite of the conductive coating some charging appeared leading to horizontal disturbances in the scans. Nevertheless the characteristic features can be explained. On the base of the EDX elemental distributions three typical areas can be distinguished: one area containing Al and O, a second containing Zr, O and Ti and a third containing Al, Ti and O. Obviously the first area is Al_2O_3 without further detectable impurities. Though EDX results cannot explain which titan phases were formed in the sample. This question can be answered by the corresponding EBSD maps in Fig. 9 taken at the same time as the EDX maps. The quality map of the detected electron backscatter patterns indicates any kind of lattice disturbances. If the disturbance due to the sample preparation is constant one finds pores, grain boundaries, twins and deformed lattices as dark regions. The lattice of the identified corundum is nearly free of deformation while the region with Al Ti and O is highly disturbed. In this region the phases TiO_2 (rutil) and Al_2TiO_4 were found by EBSD. The Zr containing areas can be identified as monoclinic ZrO_2 (Tab. 1). The EBSP quality map shows the typical twinning. There is no indication for zirconium titanates within the investigated samples.

The AZT model components were used in order to investigate interface reactions during the firing of the AZT samples. Note that there are only 2,5 vol-% of ZrO_2 and TiO_2 in the AZT composition under discussion while the interface regions of the model components exhibit the direct contact at sintering tempera-

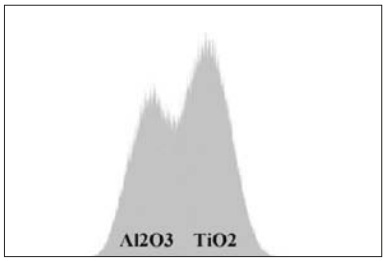

Fig. 4 Histogram of a partial volume of the AZT model component showing the absorption peaks of Al_2O_3 and TiO_2

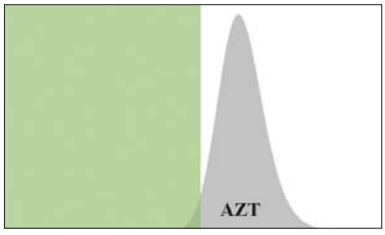

Fig. 5 Histogram of the partial volume of an AZT bending sample showing the sum absorption peak of AZT and the region dominated by cracks and pores (green)

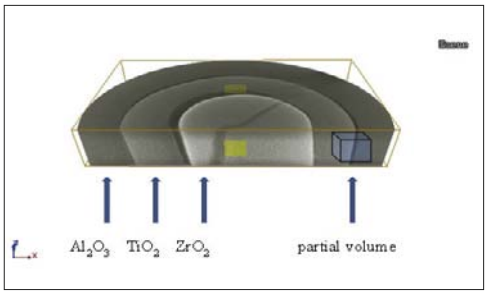

Fig. 2 XCT image of an AZT model component with a calculated cross section showing ZrO_2 in the core, TiO_2 in the middle and Al_2O_3 on the edge with cracks at the interfaces

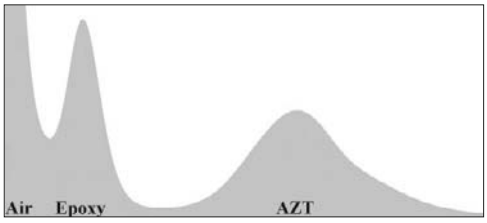

Fig. 3 Histogram of the AZT model component showing the absorption peaks of air, epoxy and AZT

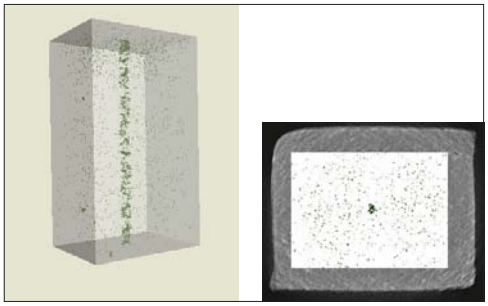

Fig. 6 Calculated 3D XCT image and corresponding cross section of a partial volume of an AZT bending sample in the as sintered state showing cracks and pores (green)

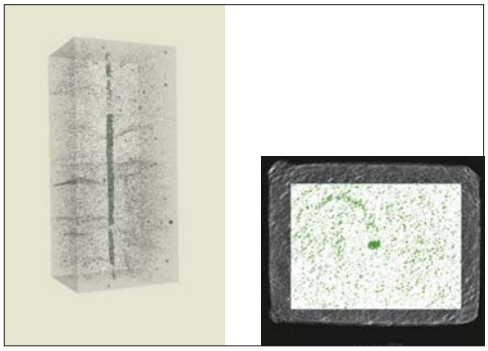

Fig. 7 Calculated 3D XCT image and corresponding cross section of a partial volume of an AZT bending sample after 5 thermo shocks showing cracks and pores (green)

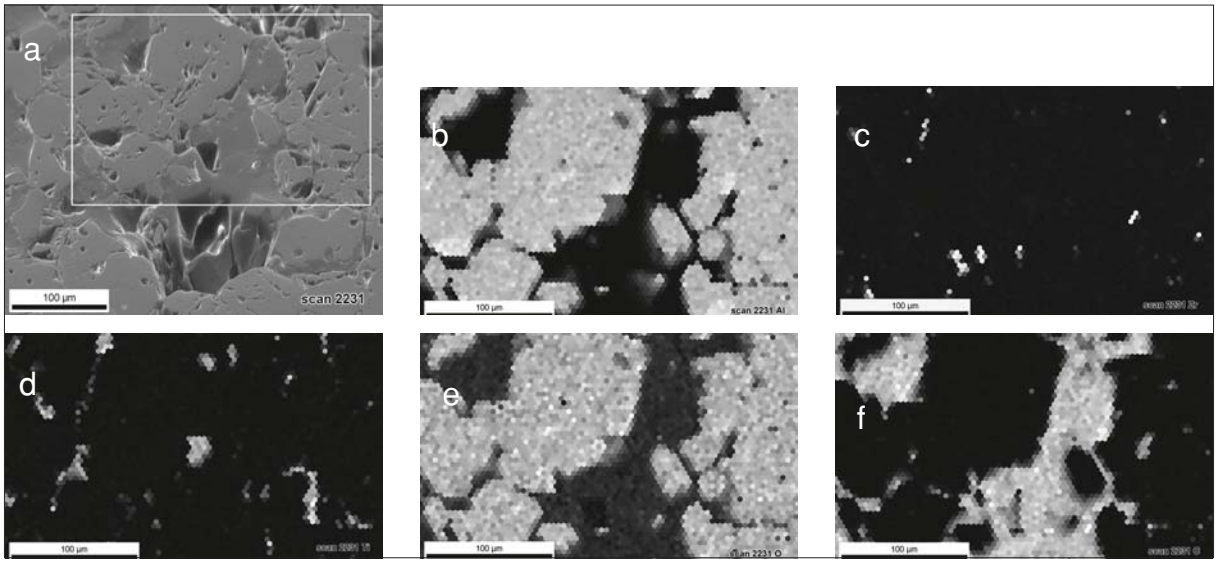

Fig. 8 SEM picture of the cross section of an AZT bending sample in the as fired state and corresponding EDX elemental distributions showing the porous region in the sample axis. a) SEI, b) Al, c) Zr, d) Ti, e) O, f) C

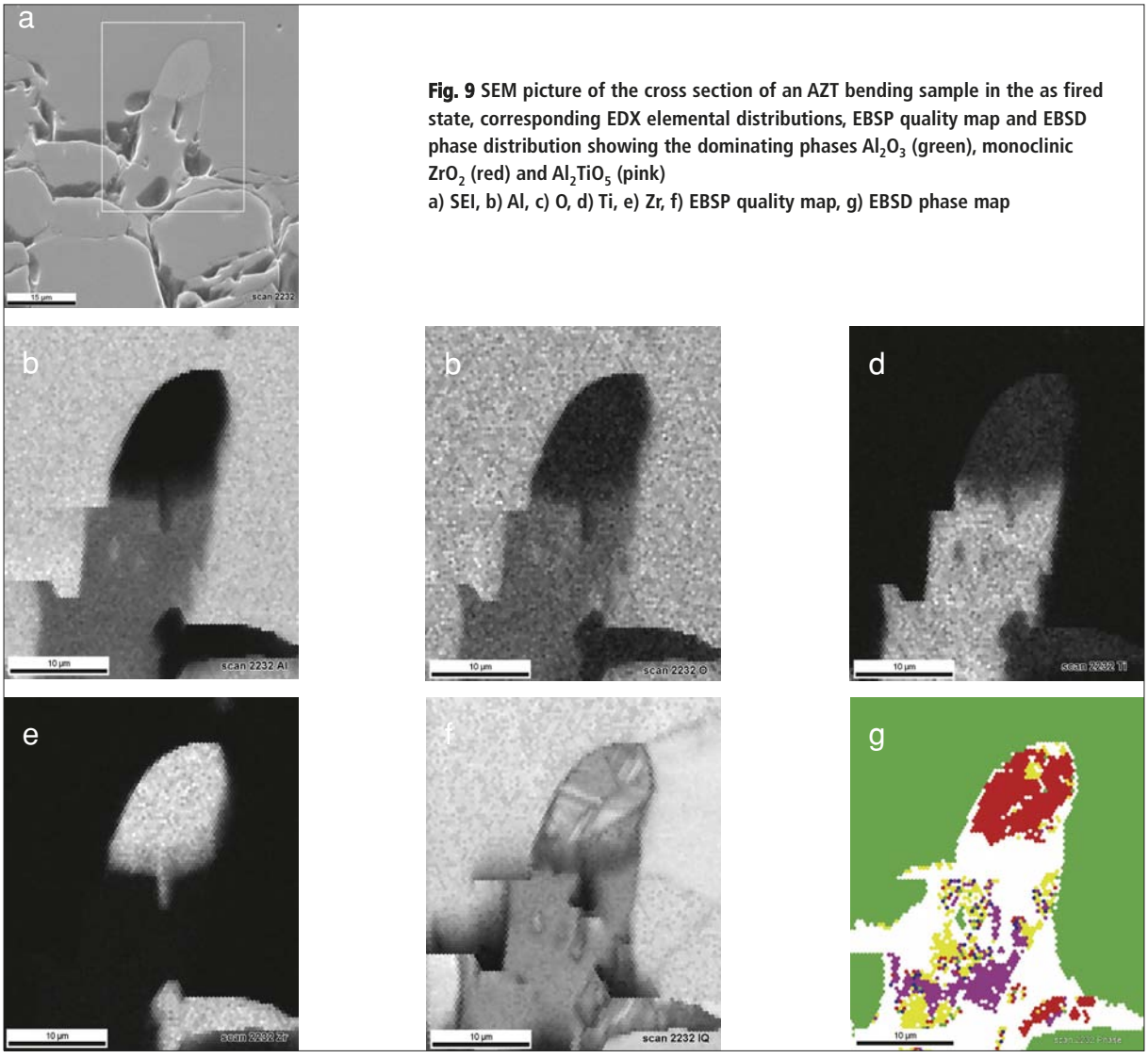

Fig. 9 SEM picture of the cross section of an AZT bending sample in the as fired state, corresponding EDX elemental distributions, EBSP quality map and EBSD phase distribution showing the dominating phases Al_2O_3 (green), monoclinic ZrO_2 (red) and Al_2TiO_5 (pink)
a) SEI, b) Al, c) O, d) Ti, e) Zr, f) EBSP quality map, g) EBSD phase map

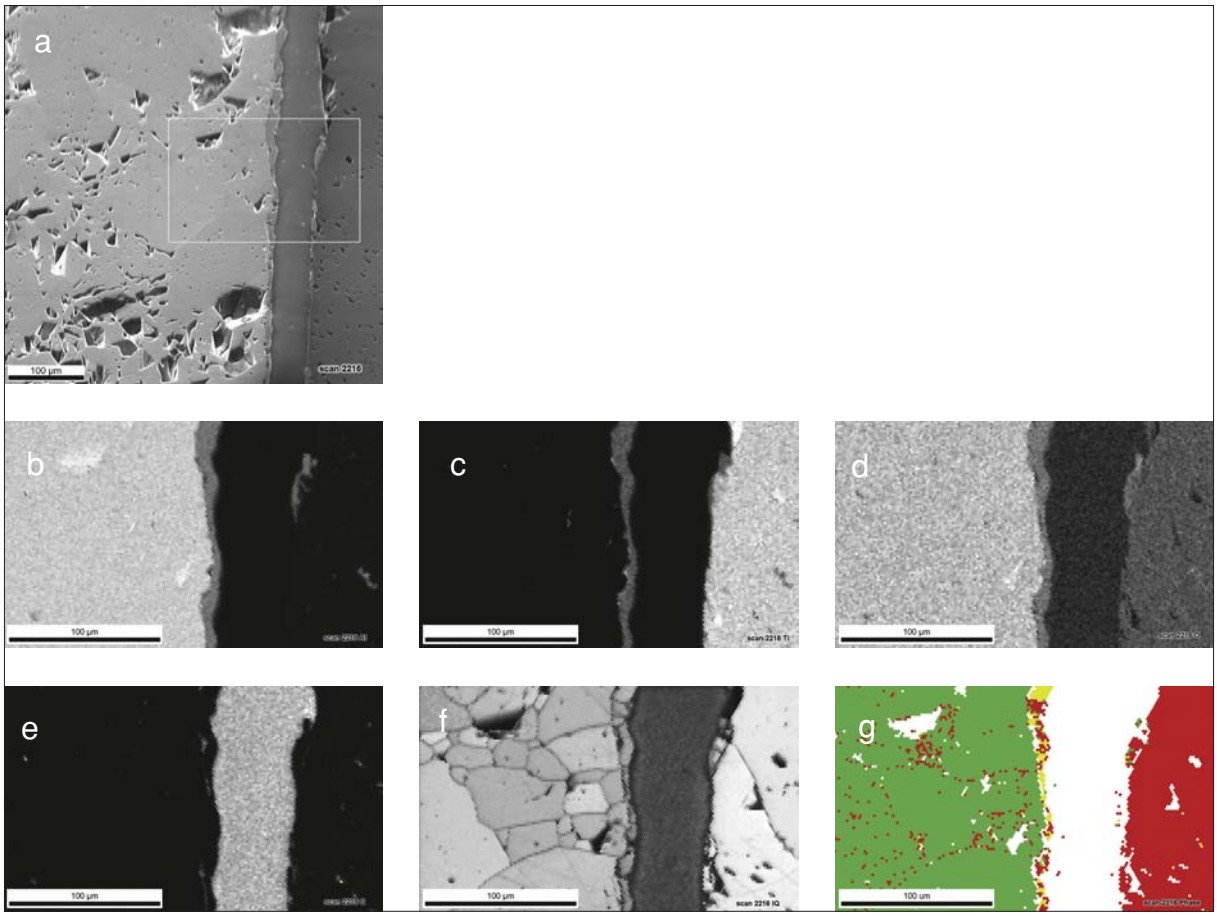

Fig. 10 Cross section of the Al_2O_3-TiO_2 interface of an AZT model component, SEM picture, corresponding EDX elemental distributions, EBSP quality map and EBSD phase distribution showing the phases Al_2O_3 (green), TiO_2 (red) and Al_2TiO_5 (yellow).
a) SEI, b) Al, c) Ti, d) O, e) C, f) EBSP quality map, g) EBSD phase map

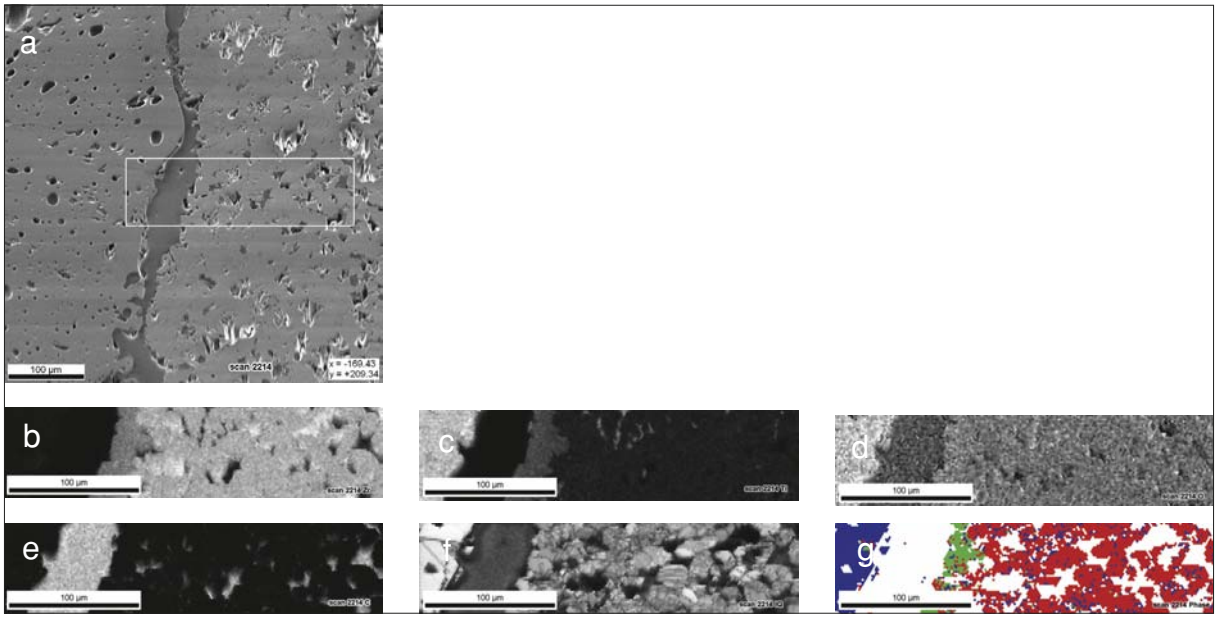

Fig. 11 Cross section of the ZrO_2-TiO_2 interface of an AZT model component, SEM picture, corresponding EDX elemental distributions, EBSP quality map and EBSD phase distribution showing the phases ZrO_2 (red), TiO_2 (blue) and $ZrTiO_4$ (green).
a) SEI, b) Zr, c) Ti, d) O, e) C, f) EBSP quality map, g) EBSD phase map

ture between ZrO_2 and TiO_2 powder on the one hand and between Al_2O_3 and TiO_2 powder on the other hand. Cross sections as indicated in Fig. 2 were cut and polished. Typical results of the EDX-EBSD investigations are given in Figs. 10 and 11.

Cracks in the order of 50 µm are observed. They are filled with epoxy as can be recognised in the EDX carbon map. These cracks are the result of cooling. Thus at sintering temperature there was a tight contact of the corresponding powder particles. Inter diffusion and phase reactions proceeded. EDX maps show that there is a reaction zone between Al_2O_3 and TiO_2. This area was identified as Al_2TiO_5 by EBSD. The lattice perfection is good as can be seen in the EBSP quality map. In the same way the formation of $ZrTiO_4$ was found at the boundary between ZrO_2 and TiO_2. The lattice perfection clearly is worse in comparison to Al_2O_3, TiO_2 and Al_2TiO_5. The same holds for ZrO_2. This is not surprising taken into account that there is always a deformation in stabilised ZrO_2. Also $ZrTiO_4$ is expected to be a metastable disordered phase [6]. The phase formation obviously proceeded on the Al_2O_3 or ZrO_2 side respectively. Thus mainly a diffusion of titanium occurred.

4 Conclusions

Newly developed AZT materials with the composition 95 – 2,5 – 2,5 exhibit excellent thermal cycling properties. In a previous work it was stated that the reason for this behaviour is the formation of micro cracks in the intra granular region between the Al_2O_3 grains. Phases with different CTE coexist. The goal of the present paper was the characterisation of these intra granular regions by XCT and EBSD. XCT investigations enable a quick overview on the structure without destroying the sample. Unfortunately the resolution is limited depending on the geometry. The X-ray attenuation coefficient depends on the atomic number and density of the materials. So also the contrast might be limited in a special case. The combination with EBSD enables new possibilities. Interesting areas within the samples can be detected by XCT. Cross sections can be calculated. These calculated cross sections can be realized in practise by metallographical preparation methods as could be shown for AZT model components. As a result one gets EBSD samples. Phase analysis can be conducted at high resolution.

The microstructures of the investigated AZT materials consist of Al_2O_3 grains and inter granular precipitations of ZrO_2, TiO_2 and Al_2TiO_5. According to [9] and [10] Al_2TiO_5 and some Ti containing phases have negative CTE and thus can help to minimize local stresses during thermal cycling. Nevertheless Al_2TiO_5 tends to decompose partially below 1200 °C. This structure leads to the excellent thermal shock performance as reported already in [11]. The additional thermal treatment after formation in means of thermal shock only reduces the amount of Al_2TiO_5. On the base of phase diagrams and the results on AZT model components the formation of $ZrTiO_4$ at sintering temperature and its stability to room temperature should be expected. This phase only was found in AZT model components on the direct contact between ZrO_2 and TiO_2 but not in the presence of Al_2O_3. One reason might be that the thermo dynamical driving force for the formation of Al_2TiO_5 is higher than for the formation of $ZrTiO_4$.

Acknowledgments

The authors would like to thank the *German Scientific Foundation (DFG)* for supporting the investigations in terms of the *Priority Program SPP 1418* "Refractory Initiative for the Reduction of Emissions – FIRE".

References

[1] Li, Y.W., Li, N., Aneziris, C.G., Hampel, M.: Physical and mechanical properties of environmental friendly carbon-bonded Al_2O_3-C refractories for sliding gate applications. cfi/Ber.DKG 82 (2005) 9, pp. E55-E59

[2] Hasselman, D.P.H.: Unified theory of thermal shock fracture initiation and crack propagation in brittle ceramics. J. Amer. Ceram. Soc. 52 (1969) 600–604

[3] Hasselman, D.P.H.: Stress resistance parameters for Brittle refractory ceramics: a compendium. Amer. Ceram. Soc. Bull. 49 (1970) 1033–1037

[4] Aneziris, C.G.; Pfaff, E.; Maier, H.R.: Ceramic materials in the system ZrO_2-TiO_2-Al_2O_3 for applications in the ferrous and non ferrous metallurgy, Key Engin. Mater. Vol. 136 (1997) 1829–1833

[5] ACerS-NIST Phase Equilibria Diagram. CD-ROM Database Version 3.2, ACerS-NIST, 2008

[6] Troitzsch, U.; Ellis, D.J.: The ZrO_2-TiO_2 phase diagram. J. of Mater. Sci. (2005) 7

[7] Wang, C.L.; et al.: The microstructure and microwave dielectric properties of zirconium titanate ceramics in the solid solution system $ZrTiO_4$-$Zr_5Ti_7O_{24}$. J. of Mater. Sci. 32 (1997) 1693–1701

[8] Kim, H.C.; et al.: Crack healing, reopening and thermal expansion behavior of Al_2TiO_5 ceramics at high temperature. J. Eur. Ceram. Soc. 27 (2007) 1431–1434

[9] Virro-Nic, P.; Pilling, J.: Thermal expansion and microstructures of melted Al_2O_3-ZrO_2-TiO_2 ceramics. J. of Mater. Sci. Letters 13 (1994) 950–954

[10] Aneziris, C.G.; Schärfl, W.; Ullrich, B.: Microstructure evaluation of Al_2O_3 ceramics with Mg-PSZ- and TiO_2-additions. J. Eur. Ceram. Soc. 27 (2007) 2191–3199

[11] Aneziris, C.G.; et al.: Thermal shock performance of fine grained Al_2O_3-ceramics with TiO_2- and ZrO_2-additions for refractory applications. Advanced Engin. Mater. 12 (2010) 478–485

[12] Baruchel, J.; et al.: X-ray tomography in material science. Paris 2000

[13] Landis, E.N.; Keane, D.T.: X-ray microtomography. Materials Characterization Vol. 61 (2010) 1305–1316

[14] Salvo, L.; et al.: X-ray micro-tomography an attractive characterisation technique in materials science. Nuclear instruments and methods in physics research. Vol. B200 (2003) 273–286

[15] Schwartz, A.J.; Kumar, M.; Adams, B.L.: Electron backscatter diffraction in materials science. New York 2000

[16] Humphreys, F.J.; et al.: Electron backscatter diffraction of grain and subgrain structures ± resolution considerations. J. of Microscopy Vol. 195 (1999) 5

[17] ICDD: ICDD PDF-2 database release 2008. International Centre for Diffraction Data (ICDD) 2008.